Available online at www.sciencedirect.com
SCIENCE DIRECT®
International Journal of Multiphase Flow 30 (2004) 481–498
International Journal of Multiphase Flow
www.elsevier.com/locate/ijmulflow

Single- and two-phase turbulent mixing rate between adjacent subchannels in a vertical 2×3 rod array channel

M. Sadatomi, A. Kawahara, K. Kano *, Y. Sumi

Department of Mechanical Engineering and Materials Science, Kumamoto University, Kurokami 2-39-1, Kumamoto 860-8555, Japan

Received 30 October 2003; received in revised form 22 February 2004

Abstract

To complete a subchannel analysis code for prediction of thermal–hydraulic behavior of a coolant in BWR fuel rod bundle, an accurate estimation of fluid transfer between subchannels is essential. Under two-phase gas–liquid flow conditions, the fluid transfer is usually subdivided into turbulent mixing, void drift and diversion cross-flow. We focused on the turbulent mixing in this study. Until now, experimental data on two-phase turbulent mixing rate have been obtained exclusively for simpler channels with two subchannels alone, and prediction methods of the mixing rates have been proposed based on such data. In order to obtain data necessary to validate the prediction methods, we newly constructed a vertical test channel simulating a BWR fuel rod bundle, which contained six rods in a rectangular array and two kinds of six subchannels. Using this channel, flow distributions and turbulent mixing rates of both gas and liquid phases were measured for single-phase water and two-phase air–water flows under a hydrodynamic equilibrium flow condition at ambient pressure. In this paper, the experimental data on turbulent mixing rates in comparison with the data for two-subchannel system at 0.34 MPa obtained by others are presented and discussed.

Keywords: Subchannel analysis; Turbulent mixing rate; Rod bundle; Hydrodynamic equilibrium flow

1. Introduction

Subchannel analysis has been used for prediction of thermal and hydraulic behavior of coolant and thus critical heat flux in a BWR fuel rod bundle. Many scientists and engineers made various

* Corresponding author.
E-mail address: keiko@mech.kumamoto-u.ac.jp (K. Kano).

0301-9322/$ - see front matter © 2004 Elsevier Ltd. All rights reserved.
doi:10.1016/j.ijmultiphaseflow.2004.03.001

trials so far in order to improve the subchannel analysis (e.g., Ninokata et al., 1997). It is necessary to properly estimate an inter-subchannel fluid transfer to improve the analysis. The fluid transfer in gas–liquid two-phase flow consists of three independent components; turbulent mixing, void drift and diversion cross-flow. As for the respective components, no decisive prediction method has been obtained yet, so their modelings are still continuing. It is therefore vital to construct and/or examine the fluid transfer models against appropriate experimental data. Concerning experiments on the fluid transfer between subchannels, two-phase turbulent mixing (Petrunik and St. Pierre, 1970; Rudzinski et al., 1972; Singh and St. Pierre, 1973) and diversion cross-flow (Tapucu, 1977; Tapucu and Merilo, 1977; Tapucu et al., 1982) have been measured using a simpler channel made up of two-subchannels (i.e., two-subchannel system). Recently, Sadatomi et al. (1994, 1995, 1996a,b, 1997), Sato et al. (1996) and Kawahara et al. (1997a,b, 1998, 2000a,b) have studied two-phase fluid transfers for hydrodynamic equilibrium and non-equilibrium flows in geometrically simple two-subchannel systems, and measured the axial distributions of both gas and liquid flow rates and void fraction in each subchannel in order to extract each component from the total fluid transfer. So far, the data on the fluid transfer have been obtained only from two-subchannel systems. However, the data obtained using a multi-subchannel system (Lahey et al., 1972; Sterner and Lahey, 1982; Yagi et al., 1992; Yadigaroglu and Maganas, 1995), similar to the system of BWR fuel element, are required to validate subchannel analysis codes. In addition, it is important that the results from the experiments in a two-subchannel system are applicable to predict the flow in a multi-subchannel system.

Regarding a multi-subchannel system, Lahey et al. (1972) measured the lateral distributions of quality and mass flux in a 3×3 rod bundle subchannel under the equilibrium flow conditions, using steam and water as the working fluids. A decade later, Sterner and Lahey (1982) obtained the data on the lateral distributions of quality and mass flux in a 2×2 rod bundle subchannel, using air and water. They reported that the air–water subchannel data had the same trend as seen in the steam–water data. Yagi et al. (1992) reported the data on void fraction distribution in a 8×8 rod bundle measured with a sophisticated X-ray scanner. Yadigaroglu and Maganas (1995) measured the lateral distributions of quality and mass flux for fully developed Refrigerant-114 two-phase flows in a three-subchannel, which were geometrically similar to corner, side and center subchannels of BWR. All the studies mentioned above are concerned with flow distribution in equilibrium flows, and are useful to validate various subchannel analysis codes. However, the experiments have been conducted under the limited flow conditions and no data have been obtained on the inter-subchannel fluids transfer.

In the present study, experiments were conducted to obtain data on turbulent mixing rates of gas and liquid phases in a multi-subchannel system under the relatively wide flow conditions. We made a new test channel with six rods in a rectangular array and six subchannels, which was designated as a 2×3 rod channel in this study. Using this system, we carried out the experiments for single-phase water and two-phase air–water flows under the hydrodynamic equilibrium flow conditions. In these experiments, the turbulent mixing rates and the fluctuations of static pressure difference between subchannels were measured. This is the first study to report the data on turbulent mixing rates in a multi-subchannel system, which is important for validation of subchannel analysis codes. We also describe the technique to measure the turbulent mixing rates in the multi-subchannel system, and compare the results with the data obtained by Rudzinski et al. (1972).

2. Experiment

2.1. Test channel and test rig

Fig. 1 shows a cross-section of a 2×3 rod channel used for the present experiment. This channel was designed to simulate to a BWR fuel rod bundle channel, and consisted of a transparent acrylic rectangular duct, two brass rods and four semi-circular acrylic rods. The brass rods were supported with 2 mm o.d. pin spacers in the central part of the duct and the semi-circular rods were glued on two opposite walls of the duct. Gap clearances between two rods and duct wall were 4 mm. To minimize the vibration of the rod, an outer diameter of the rod was enlarged to 16 mm, which was about 3.5 mm larger than that of a BWR rod. Since at least four kinds of turbulent mixing for each phase appear in an actual BWR, i.e., the mixings between corner and side, side and side, side and center, and center and center, the determination of them at once is impossible as far as we know. Therefore, we omitted the corner subchannel and simplified the channel with rod bundle to consist of symmetric two kinds of six subchannels by considering the easiness in both setting inlet flow rates in each subchannel and acquiring the data on turbulent mixing at all the gap between two subchannels. Thus, only three kinds of turbulent mixing happen: W'_{k11} between Ch.1A and 1B, W'_{k22} between Ch.2A and 2B or Ch.2CA and 2CB and W'_{k12} between Ch.1A and 2A and so on ($k = G$ for gas phase, and L for liquid phase). Cross-sectional area and hydraulic diameter of Ch.1 ($=$Ch.1A$=$Ch.1B) were 194 mm^2 and 14.3 mm, respectively. Those of Ch.2 ($=$Ch.2A$=$Ch.2B$=$Ch.2CA$=$Ch.2CB) were 138 mm^2 and 11.2 mm. Those of channel as a whole were 941 mm^2 and 12.3 mm.

Fig. 2 shows the present test rig. Water and air at atmospheric pressure and at room temperature were used as the working fluids, because it was very difficult to obtain an accurate turbulent mixing rate in a high-pressure steam–water system. The test channel was 5 m in total

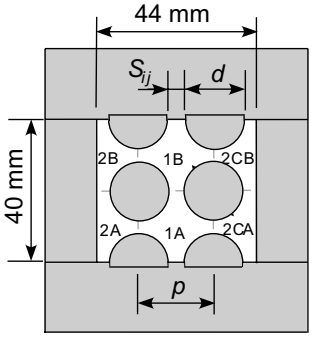

Rod diameter:
d =16mm
Rod pitch:
p = 20mm
Pitch to diameter ratio:
p/d = 1.25
Gap clearances:
$S_{11} = S_{12} = S_{22} = 4$ mm

	Ch.1	Ch.2	Whole
Hydraulic diameter [mm]	14.3	11.2	12.3
Flowarea [mm^2]	194	138	941

Fig. 1. Cross-sectional shape and dimensions of test channel.

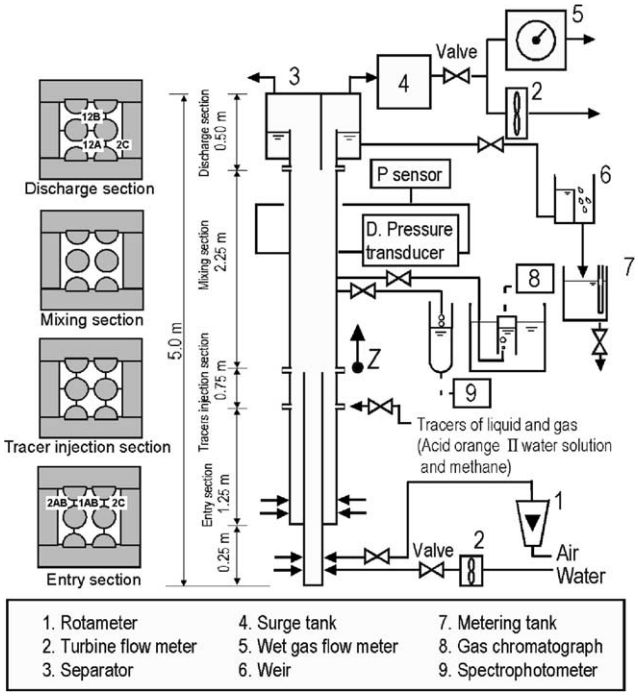

Fig. 2. Test rig.

length, and was divided into four sections from the bottom to the top, as entry (1.25 m), tracer injection (0.75 m), mixing (2.25 m) and discharge (0.5 m) sections. At the entry section, six subchannels were grouped into three, Ch.2AB, Ch.1AB and Ch.2C, as shown in the left bottom of Fig. 2. Considering the symmetry of the cross-section, we introduced the gas and the liquid at the same flow rates between subchannel groups 2AB and 2C at the inlet of the entry section. The gas and the liquid flow rates were measured with the calibrated rotameters and the turbine flow meters, respectively. At the tracer injection section, every gap between subchannels was completely closed by partitions, so the subchannels were independent. In this section, Acid orange II water solution and methane were injected into one of six subchannels as tracers for water and air, respectively, for the measurement of the turbulent mixing rate of both phases. The method to measure the turbulent mixing rates is described in Section 2.3. At the mixing section, there were no partitions between the subchannels, and inter-subchannel fluid transfer could occur. At the discharge section, six subchannels were grouped in to another three, Ch.12A, Ch.12B and Ch.2C, as shown in the left top of Fig. 2. The pressure difference among these three subchannel groups was minimized in order to realize isokinetic discharge at the inlet of the discharge section. This was done by controlling the openings of the respective valves in the air discharge lines, which were connected to three rooms of a separator. The flow rate of separated air in each subchannel group was measured with a calibrated wet gas meter or turbine flow meters, and the flow rate of water with metering tanks.

2.2. Setting of the inlet flow rate in a hydrodynamic equilibrium flow

It is convenient to measure turbulent mixing rate under a hydrodynamic equilibrium flow condition because no diversion cross-flow and void drift occur. Here, in the equilibrium flow the flow rates of both phases in every subchannel do not vary along the channel axis. Equilibrium flow does appear at a section far downstream from the inlet irrespective of the inlet flow distribution. In the present test channel, however, the length of the mixing section, 2.25 m, is insufficient for the equilibrium flow to appear. Therefore, we employed the following try-and-error method to realize the equilibrium flow.

(1) As a first trial, we introduced air and water into the three subchannel groups so that the ratio of volume flow rate of the k phase in each subchannel to that in the whole channel at the test section inlet, $Q_{k2AB}(0)/Q_k$ ($= Q_{k2C}(0)/Q_k$) and $Q_{k1AB}(0)/Q_k$, is equal to the ratio of the cross-sectional area in the corresponding subchannel to that in the whole channel.
(2) After measuring the volume flow rate of the k phase in each subchannel group at the outlet, say Q_{k12A}, we calculated the ratio of the flow rate which have to be feedbacked to the inlet.
(3) According to the calculation result from (1) and (2), the inlet flow rates in the respective subchannel groups were changed. After that, the flow rates of both phases in the whole channel were checked to be the same as those in the first step.
(4) This procedure was repeated until the ratios at the test section inlet and the outlet were sufficiently close in each subchannel. Finally, when these ratios became close enough (within ±1%), we adopted these values as the ratios at a hydrodynamic equilibrium flow.

2.3. Measurement of turbulent mixing rate

Turbulent mixing rates of gas and liquid phases between subchannels, W'_{k11}, W'_{k12}, W'_{k22} ($k = G$ for gas, L for liquid) were measured with a tracer technique (Sadatomi et al., 1995). Firstly, tracers (methane and acid orange II water solution) were injected into Ch.1A or Ch.1B in the tracer injection section. Small amounts of gas and liquid containing the tracers were extracted from Ch.1A, Ch.1B, Ch.2A and Ch.2B at more than three axial positions in the mixing section. In order

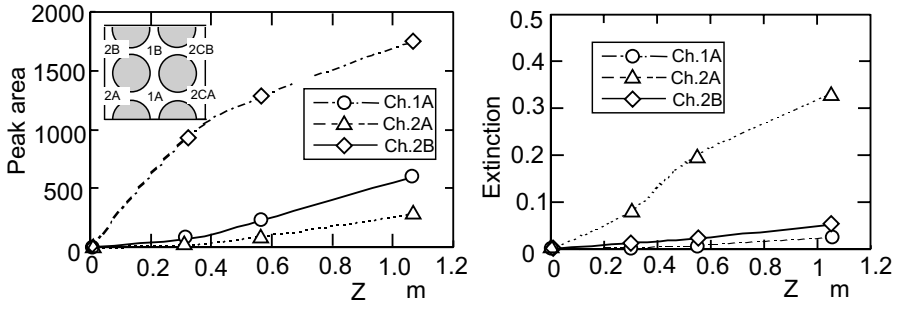

Fig. 3. Tracer concentration distribution in the axial direction at $j_L = 0.2$ m/s and $j_G = 35$ m/s.

to determine tracer concentrations of gas and liquid in each position, the gas and the liquid samples were fed to a gas chromatograph and a spectrophotometer, respectively. Since the value of peak area detected by the gas chromatograph was proportional to the concentration of methane and that of extinction by the spectrophotometer to that of acid orange II, we determined the respective concentrations from the peak area and the extinction. Fig. 3(a) and (b) show typical distributions of the peak area and the extinction, i.e., gas and liquid tracer concentrations, along the channel axis for an annular flow when the tracers were injected into Ch.1B in the tracer injection section. The ordinate in Fig. 3(a) is the peak area for the gas tracer, while that in Fig. 3(b) the extinction for the liquid one. The abscissa is the distance from the inlet of the mixing section, Z. The tracer concentrations in Ch.1A, Ch.2A and Ch.2B, un-injected subchannels alone are shown as a representative. Similar results were obtained from Ch.2A and Ch.2CA, and Ch.2B and Ch.2CB (data not shown), which was considered to be due to the symmetry of the flow in the channel. The agreement of these data between Ch.2A and Ch.2CA was within ±1.4% for the liquid phase and ±3.5% for the gas phase, and that between Ch.2B and Ch.2CB was with in ±5.4% and ±1.3% for the respective phases. The tracer concentrations in Ch.1A, Ch.2A and Ch.2B increased with Z due to the turbulent mixing. Substituting the tracer concentration data, we calculated W'_{k12} as indicated below.

$$W'_{k12} = \frac{\dot{m}_{k1A}A_{1A}\dot{m}_{k2B}A_{2B}}{(Z_2 - Z_1)(\dot{m}_{k1A}A_{1A} + 2\dot{m}_{k2B}A_{2B})} \ln\left\{\frac{C_{k1A}(Z_1) + C_{k1B}(Z_1) - C_{k2B}(Z_1) - C_{k2A}(Z_1)}{C_{k1A}(Z_2) + C_{k1B}(Z_2) - C_{k2B}(Z_2) - C_{k2A}(Z_2)}\right\} \quad (1)$$

Here $\dot{m}_{k1A}$ is the k-phase mass flux in Ch.1A, $C_{k1A}(Z_1)$ the k-phase tracer concentration in Ch.1A at an axial position Z_1, A_{1A} the cross-sectional area of Ch.1A. Eq. (1) was derived from a conservation equation of a tracer mass by assuming W'_{k12} ($= W'_{k1A2A} = W'_{k1B2B} = W'_{k1A2CA} = W'_{k1B2CB}$) to be constant along the channel axis as shown in Appendix A.

Secondly, the tracers were injected into one of the four subchannels, Ch.2A, Ch.2B, Ch.2CA and Ch.2CB. Similarly, we obtained the tracer concentrations data along the channel axis. With the tracer concentration data and W'_{k12}, W'_{k22} was calculated as follows.

$$W'_{k22} = \frac{1}{2}\left[-W'_{k12} + \frac{\dot{m}_{k2B}A_{2B}}{Z_2 - Z_1} \ln\left\{\frac{C_{k2A}(Z_1) - C_{k2B}(Z_1) + C_{k2CB}(Z_1) - C_{k2CA}(Z_1)}{C_{k2A}(Z_2) - C_{k2B}(Z_2) + C_{k2CB}(Z_2) - C_{k2CA}(Z_2)}\right\}\right] \quad (2)$$

Finally, W'_{k11} was indirectly determined by the following trial-and-error method. Using W'_{k12}, W'_{k22} data, and an assumed value of W'_{k11}, we calculated tracer concentration distributions along the channel axis for all the subchannels when the tracers were injected into Ch.1B or one of Ch.2A, Ch.2B, Ch.2CA and Ch.2CB. In the calculation, we used a conservation equation of a tracer mass accounting for the effects of turbulent mixing. Similar calculations were repeated by changing W'_{k11} value. When the calculated data corresponded to the experimental data best, the W'_{k11} value was chosen to use as the experimental data.

2.4. Measurement of fluctuations of static pressure difference between subchannels

In order to study the relationship between the turbulent mixing rate and the fluctuations of static pressure difference between the subchannels i and j, the fluctuations of the pressure difference, $\Delta P_{ij}(t)$, were measured in the present multi-subchannel system as described in the study by

Kawahara et al. (1997a). $\Delta P_{ij}(t)$ at $Z = 1550$ mm in the mixing section was measured with a differential pressure transducer with a resonance frequency of about 3–5 kHz. Analog signals from the transducer were sampled at 1 kHz with an A/D converter, and the resulting digital data were processed by a computer. A root-mean-square value was calculated by the following equation.

$$\Delta P'_{ij,\mathrm{RMS}} = \sqrt{\frac{1}{T}\int_0^T \{\Delta P_{ij}(t) - \Delta P_{\mathrm{ave}}\}^2 \,\mathrm{d}t} \tag{3}$$

Here, T is the predetermined time interval for the processing (20 s in this study), $\Delta P_{ij}(t)$ the static pressure difference at an arbitrary time, t, and ΔP_{ave} the average of the pressure difference over the time interval, T. ΔP_{ave} value in reality was very close to zero in an equilibrium flow.

In addition, the fluctuations of static pressure in each subchannel were also measured as a reference.

2.5. Experimental conditions

Fig. 4 shows flow conditions. The ordinate and the abscissa indicate the superficial velocities for liquid and gas, respectively, as a whole channel. Two broken lines represent the flow pattern transition lines, determined from the correlation for bubble flow to slug flow transition (Taitel et al., 1980), and the correlation for churn flow to annular flow transition (Golan and Stenning, 1969). According to the observation of the flow with a high-speed video camera, these transition lines agreed substantially with those observed in Ch.2 (see Appendix B). Therefore, we assumed that these lines would agree with those in Ch.1, because the observation of the flow in Ch.1 was not possible due to the arrangement of the rods. Open circles on $j_G = 0$ indicate the data from the single-phase water flow experiments. Closed circles indicate flow conditions in which both gas and liquid data were taken, and open circles indicate where only liquid data were collected. Experimental conditions are summarized as follows: In single-phase water flow, the range of mean water velocity was $u_L = 0.7$–2.0 m/s; In two-phase flow, the range of superficial velocity was $j_G = 0.1$–35

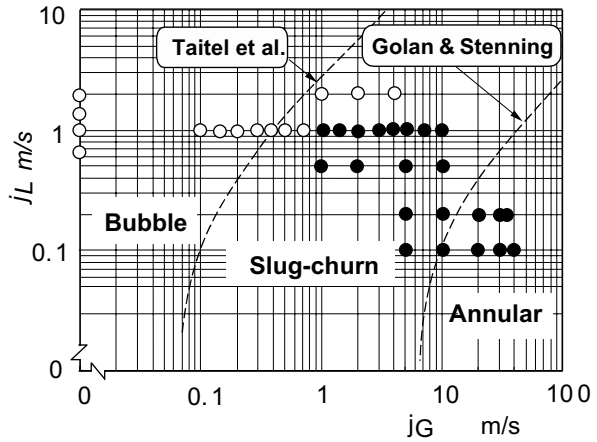

Fig. 4. Flow conditions (●: both gas and liquid data were taken, ○: liquid data alone).

m/s, and $j_L = 0.1$–2.0 m/s for gas and liquid respectively. The flow patterns covered in two-phase flow were bubble, slug–churn, and annular flows.

3. Result and discussion

3.1. Turbulent mixing rate in single-phase water flow

The W'_{ij}/μ vs. Re_{ij} coordinate system is widely used to correlate turbulent mixing rate data in the single-phase flow, and the correlations based on this system are known to be applicable for variety of fluids (Sadatomi et al., 1996b). Fig. 5 shows the data obtained from the single-phase water flow experiments. Data points are marked with different symbols according to two relating subchannels. The ordinate is the dimensionless mixing rate, W'_{ij}/μ, and the abscissa the Reynolds number defined as

$$Re_{ij} = \frac{\rho u_{ij} D_{hij}}{\mu} \tag{4}$$

where

$$u_{ij} = \frac{u_i A_i + u_j A_j}{A_i + A_j} \tag{5}$$

Here, u and A are the mean velocity and the cross-sectional areas, the subscription i, j indicate Ch.i and Ch.j, ρ and μ the density and viscosity of the fluid. D_{hij} in Eq. (4) is the hydraulic diameter of an imaginary channel with subchannels, Ch.i and Ch.j. Measured values of W'_{ij}/μ increase with Re_{ij}, and W'_{12}/μ is about 20% higher than others. Three lines, calculated from Sadatomi et al.'s model (Sadatomi et al., 1996b), agree reasonably with the data within 26%, except for one data points asterisked at the lowest Reynolds number.

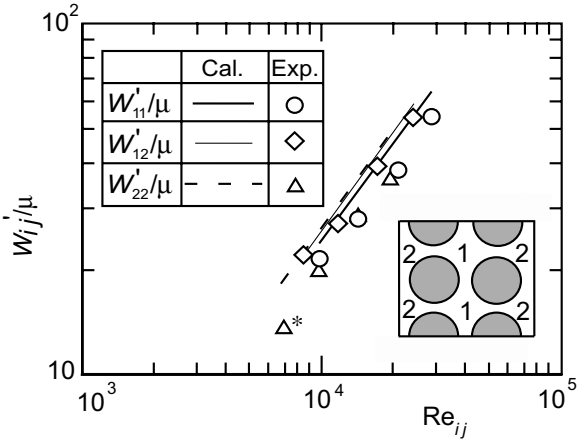

Fig. 5. Turbulent mixing rate against Reynolds number for single-phase water flow.

3.2. Turbulent mixing rates in two-phase flow

3.2.1. Turbulent mixing rate

Fig. 6(a) and (b) show the liquid and the gas turbulent mixing rates, respectively, obtained from two-phase flow experiments. The abscissa in both figures indicate the superficial gas velocity of two relating subchannels, j_{Gij} $(=(j_{Gi}A_i + j_{Gj}A_j)/(A_i + A_j))$. Experimental data were obtained by changing superficial gas velocity in the whole channel, j_G, at a fixed liquid velocity, j_L. Data points at $j_G = 0$ in Fig. 6(a) indicate single-phase water flows. Different symbols were used to indicate different relating subchannel and j_L. Flow pattern boundaries are shown according to the method by Taitel et al. (1980) for the flows at $j_L = 1.0$ m/s. In bubble flow, the liquid mixing rate, W'_{Lij}, was nearly the same as that for single-phase water flow. At the transition point from bubble flow to slug–churn flow ($j_G \cong 0.5$ m/s), W'_{Lij} drastically increased the level to about four times higher than that of the single-phase water flow. After that, W'_{Lij} stayed almost constant, and then decreased as j_G increased. Turbulent mixing rates of gas phase in bubble flow could not be obtained, since variation in tracer concentrations along the channel axis was too small to obtain turbulent mixing data with enough accuracy. In the transition region from bubble flow to slug–churn flow, the gas mixing rate, W'_{Gij}, drastically increased. In slug or churn flow, W'_{Gij} became about 10 times higher than that of the single-phase air flow shown by a broken line in Fig. 6(b), and gradually decreased as j_G increased. In annular flow, the gas phase turbulent mixing rate is considered to be close to that for single-phase air flow. Therefore, some W'_{Gij} data, which is much lower than those for single-phase air flow, seem inaccurate. As mentioned in Section 2.3, W'_{k11} were indirectly obtained

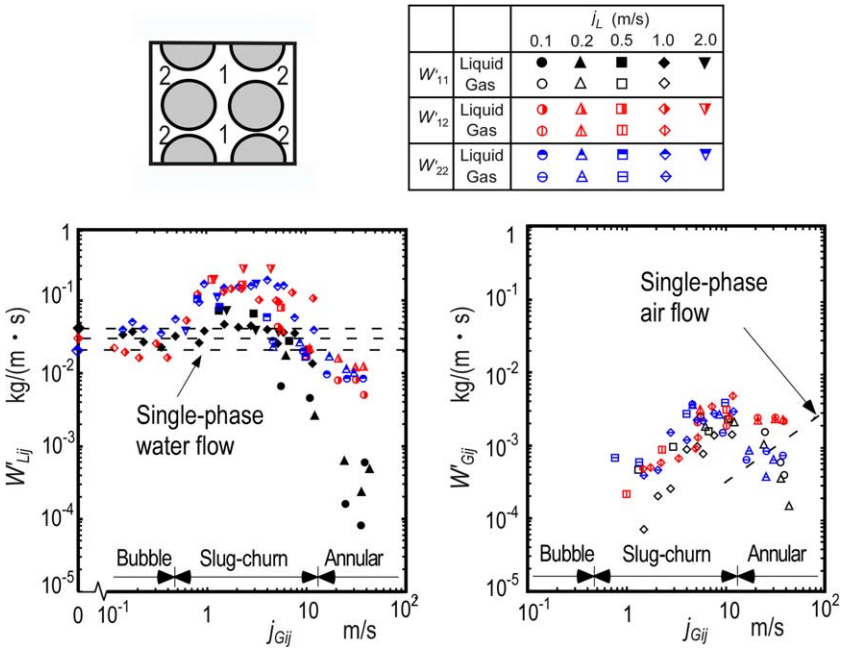

Fig. 6. Turbulent mixing rate for each phase in two-phase flow against mean superficial gas velocity between adjacent subchannels.

by using W'_{k22} and W'_{k12} data. Therefore, W'_{k11} data became inaccurate in comparison with W'_{k22} and W'_{k12}, and showed large scatter. Contrary to this, W'_{k22} and W'_{k12} are more reliable, and became close to the value in single-phase air flow as j_G increased.

Figs. 7 and 8 show the cross-sectional shape and the dimensions of the square-array channel used by Rudzinski et al.'s (1972), and their data on turbulent mixing rates at the total mass fluxes of $\dot{m} = 0.68 \times 10^3$ and 1.08×10^3 kg/(m^2 s), respectively. This channel is similar in shape to Ch.1-1 in the present study, but has a narrow gap clearance. They measured turbulent mixing rates of the air and the water in two-phase flows at a system pressure of 0.34 MPa (absolute). In Fig. 8, the mean void fraction, ε_{Gij}, defined as

$$\varepsilon_{Gij} = \frac{\varepsilon_{Gi}A_i + \varepsilon_{Gj}A_j}{A_i + A_j} \tag{6}$$

was chosen as the abscissa, instead of the mean quality as in their original paper, which would make it easier to compare with the data obtained under different pressure conditions. (Sadatomi et al., 1995) In Eq. (6), ε_{Gi} and ε_{Gj} are the void fractions in Ch.i and Ch.j, respectively, calculated from Chisholm's correlation (Chisholm, 1973) by substituting gas and liquid flow rates in each subchannel. In Fig. 8 Rudzinski et al.'s data can be well represented by the two solid curves for the liquid phase and the gas phase, irrespective of the difference in the mass flux. Rudzinski et al.'s

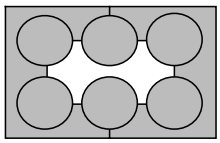

Rod diameter	20.8 mm
Hydraulic diameter	8.8 mm
Cross-sectional area	152.4 mm^2
Gap clearance	0.89 mm
Pitch/rod diameter ratio	1.04
Interconnection length	1524 mm

Fig. 7. Cross-section and dimensions of square array channel used by Rudzinski et al. (1972).

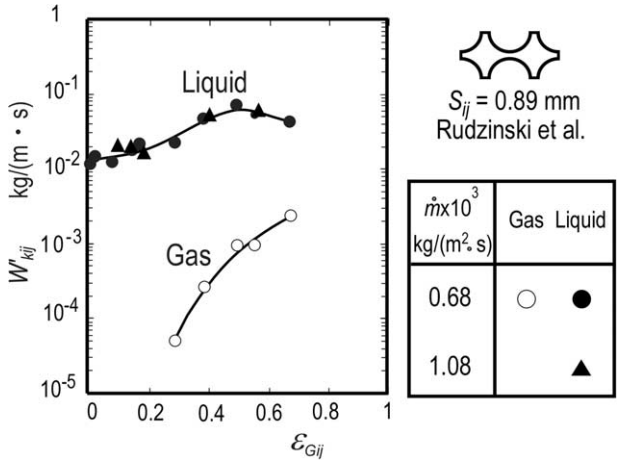

Fig. 8. Turbulent mixing rates by Rudzinski et al. (1972).

data in two-subchannel system, as representative, are compared with the present data in multi-subchannel system.

Fig. 9 compares Rudzinski et al.'s data with W'_{k11} between Ch.1A and Ch.1B (i.e., Ch.1-1). The abscissa indicates the mean void fraction between two relating subchannels, ε_{Gij}, defined as Eq. (6). Our data showed a similar trend to the data by Rudzinski et al. over $\varepsilon_{Gij} < 0.7$, suggesting that the mechanism of turbulent mixing is similar in both channels at the same void fraction. In addition, it is very interesting that the mixing rate in Ch.1-1 was nearly the same as that in Rudzinski et al.'s channel in liquid phase, and was about half of Rudzinski et al.'s data in gas phase, though the gap clearance in the present channel was four times of that in Rudzinski et al.'s channel. The reason for this quantitative difference is not known at present.

Fig. 10 compares W'_{k11} and W'_{k22} in our study, remains to be elucidated with Rudzinski et al.'s data. Both W'_{k11} and W'_{k22} data showed similar trend to Rudzinski et al.'s data. The most interesting feature is that W'_{k11} was smaller than W'_{k22}, particularly in slug–churn flow, though the flow rates of both phases in Ch.1 were always larger than those in Ch.2. The probable reason is as follows: In slug–churn flow, fluctuations of the static pressure difference between adjacent subchannels due to the passage of slugs in the respective subchannels were smaller in Ch.1-1 than Ch.2-2 (see Section 3.2.2); This caused smaller mixing rate in Ch.1-1 because the major component of turbulent mixing rate in slug–churn flow is due to the fluctuations of static pressure difference, as clarified by Kawahara et al. (1997a,b, 2000b). In annular flow, W'_{L11} was smaller than W'_{L22}. The reason is that liquid film at the gap in Ch.1-1 became thinner than that in Ch.2-2, and liquid mixing mainly occurred in liquid film rather than in liquid entrainment in the gas core. The gas mixing rate in annular flow, on the other hand, W'_{G11} was larger than W'_{G22}. This may be due to the fact that W'_{G11} increased with both gas fraction and inherent gas turbulence in the gap.

Fig. 11 shows a comparison between W'_{k22} and W'_{k12}. Both W'_{k22} and W'_{k12} showed similar trend to Rudzinski et al.'s data, but the liquid mixing rate was roughly five times larger than Rudzinski et al.'s data. Furthermore, W'_{k12} and W'_{k22} were nearly the same for both phases especially in slug–churn flow. The reason of this is also that the mixing rate in this regime depends on the intensity

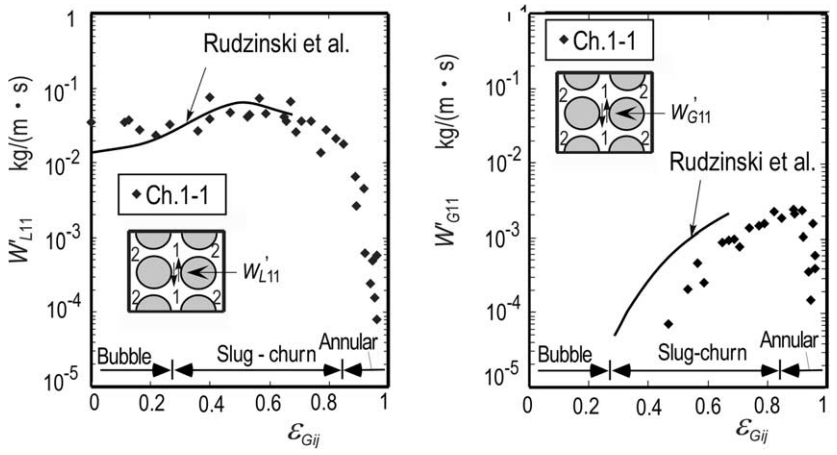

Fig. 9. Turbulent mixing rate of each phase between Ch.1-1 against mean void fraction between related subchannels (comparison of Rudzinski et al.'s data with the present ones).

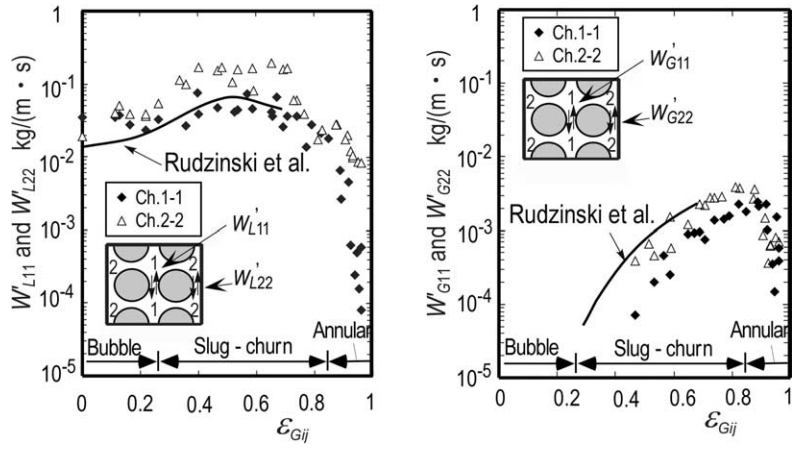

Fig. 10. Comparison of W'_{k11} and W'_{k22} (comparison of Rudzinski et al.'s data with the present ones).

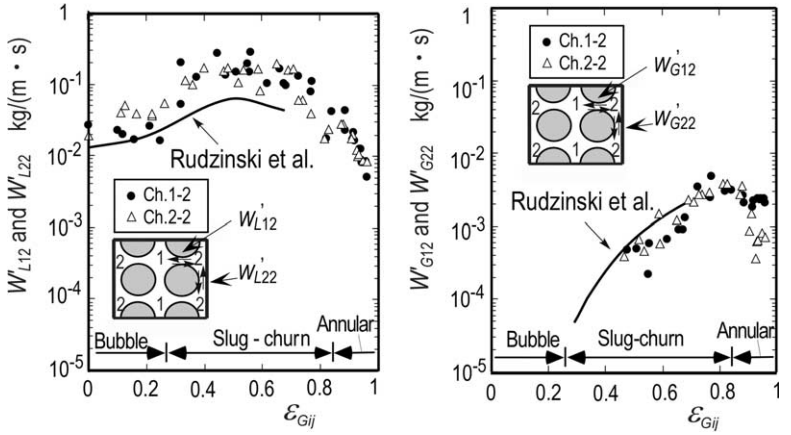

Fig. 11. Comparison of W'_{k12} and W'_{k22} (comparison of Rudzinski et al.'s data with the present ones).

of the fluctuations of pressure difference between subchannels (Fig. 12). In annular flow, gas phase mixing rate in Ch.1-2 was a little larger than W'_{G22}. The reason may be similar when $W'_{G11} > W'_{G22}$.

3.2.2. Fluctuations of static pressure difference between subchannels

Kawahara et al. (1997a,b, 2000b) have reported in their studies on two-phase turbulent mixing in a two-subchannel system that the instantaneous pressure difference between the subchannels, $\Delta P_{ij}(t)$, especially in slug–churn flow causes a good deal of fluid transfer between subchannels. In addition, they showed that the variation of $\Delta P'_{ij,\mathrm{RMS}}$, root-mean-square values of $\Delta P_{ij}(t)$ over a long time interval, with the mean void fraction, ε_{Gij}, has a similar trend to that of the liquid phase turbulent mixing rate, W'_{Lij}. Therefore, we obtained the experimental data on $\Delta P'_{ij,\mathrm{RMS}}$ were obtained for three different subchannel combinations, i.e., Ch.1-1, Ch.1-2, and Ch.2-2 in the present study (Fig. 12). A similar trend was observed in the present experiment

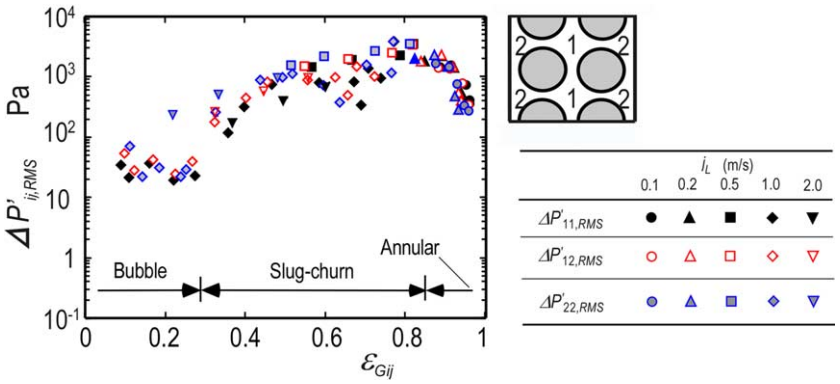

Fig. 12. RMS value of fluctuations of pressure difference between subchannels against void fraction.

and the previous experiment using a two-subchannel system (Kawahara et al., 1997a,b); In bubble flow, $\Delta P'_{ij,\mathrm{RMS}}$ was close to the value of single-phase water flow. At the transition from bubble flow to slug flow, $\Delta P'_{ij,\mathrm{RMS}}$ drastically increased and became nearly constant in slug–churn flow irrespective of ε_{Gij}. In annular flow, $\Delta P'_{ij,\mathrm{RMS}}$ gradually decreased with increasing of ε_{Gij}. This trend is quite similar to that of the turbulent mixing rate of the liquid phase. A comparison of $\Delta P'_{ij,\mathrm{RMS}}$ among the subchannel combinations showed that $\Delta P'_{ij,\mathrm{RMS}}$ of Ch.1-1 was lower than those of Ch.2-2 and Ch.1-2, corresponding to the relation of $W'_{k11} < W'_{k22}$ and W'_{k12} in Figs. 10 and 11. These results indicate that turbulent mixing rate in the 2×3 rod channel should be predicted by taking account of the effects of $\Delta P'_{ij,\mathrm{RMS}}$ in a similar manner for the two-subchannel system (Kawahara et al., 1997a, 2000b).

In slug–churn flow in the 2×3 rod channel, there were relatively smaller Taylor bubbles occupying one of the six subchannels and larger ones occupying both of the central subchannels. The smaller bubbles were independent of each other in the respective subchannels and flowed at random, therefore the passage of the smaller ones caused considerable pressure differences between the subchannels. The larger bubbles, on the other hand, did not cause larger pressure differences. Thus, the passage of the smaller bubbles enhances the turbulent mixing between the subchannels, while that of the larger ones does not enhance the mixing between the central subchannels. This is why the relations of $\Delta P'_{11,\mathrm{RMS}} < \Delta P'_{22,\mathrm{RMS}}$ and $W'_{k11} < W'_{k22}$ hold.

4. Conclusions

In order to obtain experimental data to validate the subchannel analysis codes, we made a new vertical test channel with six rods in a rectangular array and six subchannels, i.e., 2×3 rod channel, and conducted experiments in single-phase water and two-phase air–water flows under the hydrodynamic equilibrium flow conditions at ambient pressure and temperature. The turbulent mixing rates of gas and liquid phases and the fluctuations of static pressure difference between subchannels were measured. This is the first study to report the data on the turbulent mixing rate in a multi-subchannel system, so must be useful to examine existing turbulent mixing models. The main findings are as follows.

(1) Similarity of trend between the liquid-phase mixing rate and the pressure difference fluctuations data was confirmed also for the present multi-subchannel system, as was confirmed for two-subchannel system (Kawahara et al., 1997a).
(2) The present turbulent mixing rates data and Rudzinski et al.'s data in two-subchannel system at 0.34 MPa showed a similar trend, depending on two-phase flow pattern over a void fraction range of $\varepsilon_{Gij} < 0.7$. This suggests that the mechanism of the turbulent mixing is similar in these channels at the same void fraction.

As a future work, we are planning to examine some existing turbulent mixing models against the present data to check their applicability in a multi-subchannel system.

Acknowledgements

We would like to thank Messrs. T. Hirayama and Y. Miyazaki, who were students at Kumamoto University, for their helps with the experiments. This work was supported by the grant from the Institute of Applied Energy (IAE), Ministry of Economy, Trade and Industry (METI), Japan.

Appendix A. Derivation of equations to determine the turbulent mixing rates, W'_{k12}

In the 2×3 rod channel, the turbulent mixing occurs through the seven gaps as shown in Fig. 13. Due to the symmetry of the flow in the channel, they are divided into three groups:

$$W'_{k11} = W'_{k1A1B} \tag{A.1}$$

$$W'_{k12} = W'_{k1A2A} = W'_{k1B2B} = W'_{k1A2CA} = W'_{k1B2CB} \tag{A.2}$$

$$W'_{k22} = W'_{k2A2B} = W'_{k2CA2CB} \tag{A.3}$$

Here, the derivation of Eq. (1) in Section 2.3 to determine the W'_{k12}, is shown below as an example.

In a subchannel analysis, the transfer of a tracer mass from the subchannel i to j due to the turbulent mixing over an axial length, dZ, is expressed as

$$m'_{ij} = W'_{ij}(C_i - C_j)\,dZ \tag{A.4}$$

Here, C_i and C_j are the concentrations of tracer in subchannel i and j, respectively. Considering of the mass transfer in Eq. (A.4) yields the conservation equations of tracer mass for each subchannel in the 2×3 rod channel.

For Ch.1A

$$C_{k1A}\dot{m}_{k1A}A_{1A} - W'_{k11}(C_{k1A} - C_{k1B})\,dZ - W'_{k12}(C_{k1A} - C_{k2A})\,dZ - W'_{k12}(C_{k1A} - C_{k2CA})\,dZ - (C_{k1A} + dC_{k1A})\dot{m}_{k1A}A_{1A} = 0 \tag{A.5}$$

For Ch.1B

$$C_{k1B}\dot{m}_{k1B}A_{1B} - W'_{k11}(C_{k1B} - C_{k1A})\,dZ - W'_{k12}(C_{k1B} - C_{k2B})\,dZ - W'_{k12}(C_{k1B} - C_{k2CB})\,dZ - (C_{k1B} + dC_{k1B})\dot{m}_{k1B}A_{1B} = 0 \tag{A.6}$$

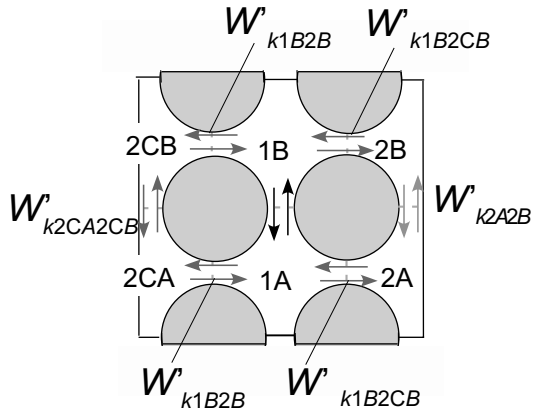

Fig. 13. Seven kinds of turbulent mixing thorough the seven gaps between subchannels.

For Ch.2A

$$C_{k2A}\dot{m}_{k2A}A_{2A} - W'_{k12}(C_{k2A} - C_{k1A})\,dZ - W'_{k22}(C_{k2A} - C_{k2B})\,dZ - (C_{k2A} + dC_{k2A})\dot{m}_{k2A}A_{2A} = 0 \tag{A.7}$$

For Ch.2B

$$C_{k2B}\dot{m}_{k2B}A_{2B} - W'_{k12}(C_{k2B} - C_{k1B})\,dZ - W'_{k22}(C_{k2B} - C_{k2A})\,dZ - (C_{k2B} + dC_{k2B})\dot{m}_{k2B}A_{2B} = 0 \tag{A.8}$$

For Ch.2CA

$$C_{k2CA}\dot{m}_{k2CA}A_{2CA} - W'_{k12}(C_{k2CA} - C_{k1A})\,dZ - W'_{k22}(C_{k2CA} - C_{k2CB})\,dZ - (C_{k2CA} + dC_{k2CA})\dot{m}_{k2CA}A_{2CA} = 0 \tag{A.9}$$

For Ch.2CB

$$C_{k2CB}\dot{m}_{k2CB}A_{2CB} - W'_{k12}(C_{k2CB} - C_{k1B})\,dZ - W'_{k22}(C_{k2CB} - C_{k2CA})\,dZ - (C_{k2CB} + dC_{k2CB})\dot{m}_{k2CB}A_{2CB} = 0 \tag{A.10}$$

Here, $\dot{m}$ is the mass flux, A the flow area. In a hydraulically equilibrium flow, the flow rates in the respective subchannels must satisfy the next equations.

$$\dot{m}_{k1A}A_{1A} = \dot{m}_{k1B}A_{1B} \tag{A.11}$$

$$\dot{m}_{k2A}A_{2A} = \dot{m}_{k2B}A_{2B} = \dot{m}_{k2CA}A_{2CA} = \dot{m}_{k2CB}A_{2CB} \tag{A.12}$$

If we inject the tracer into Ch.1A or Ch.1B,

$$C_{k2A} = C_{k2CA} \quad \text{and} \quad C_{k2B} = C_{k2CB} \tag{A.13}$$

Rearranging Eqs. (A.5)–(A.13), and integrating the resulting equation assuming W'_{k12}, we obtained:

$$W'_{k12} = \frac{\dot{m}_{k1A}A_{1A}\dot{m}_{k2B}A_{2B}}{(Z_2 - Z_1)(\dot{m}_{k1A}A_{1A} + 2\dot{m}_{k2B}A_{2B})} \ln\left\{\frac{C_{k1A}(Z_1) + C_{k1B}(Z_1) - C_{k2B}(Z_1) - C_{k2A}(Z_1)}{C_{k1A}(Z_2) + C_{k1B}(Z_2) - C_{k2B}(Z_2) - C_{k2A}(Z_2)}\right\}. \quad (A.14)$$

Appendix B. Flow observation

The observation of the flows in the 2×3 rod channel was made with a high speed video camera or a digital camera from two directions as shown in Fig. 14. Fig. 15(a) and (b) are the typical photographs showing the bubble and the slug–churn flows at $j_L = 0.5$ m/s, each under the hydraulically equilibrium flow condition. Paired pictures from the side and the front are

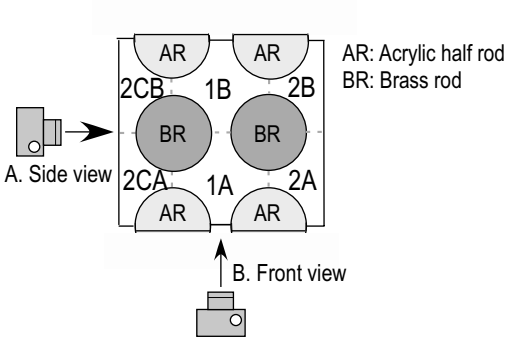

Fig. 14. Arrangement of two cameras for flow pattern observation.

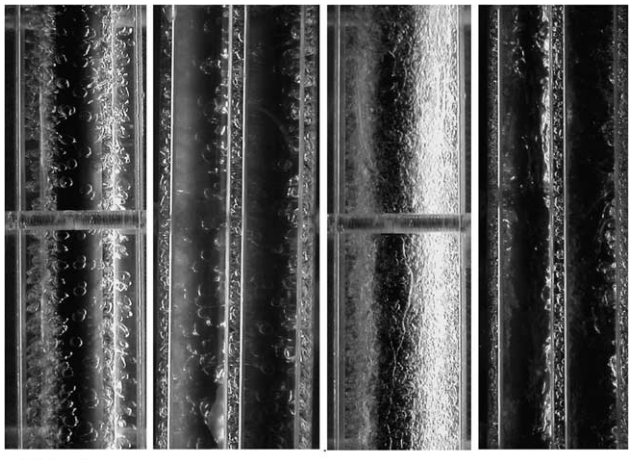

Fig. 15. Typical flows at $j_L = 0.5$ m/s under hydraulically equilibrium flow condition.

shown in each flow. The flow pattern in Ch.2 was mainly observed from the side view, and the flow pattern in Ch.1 from the front view. The picture from the front is vague due to the lens effects of the acrylic half rod. Similar paired pictures were taken for other flow conditions. From these pictures, the flow pattern in Ch.2 was confirmed to agree with that for simpler geometries like a circular pipe. As to the flow pattern in Ch.1, it appeared similar to that in Ch.2. In bubble flow regime, the size and the density of small bubbles were similar between Ch.1 and Ch.2, and the size became smaller as j_L increased. In slug and churn flow regimes, the large shroud Taylor bubble occupying all the subchannels, observed in stagnant water test by Venkateswara et al. (1982), did not appear, but the cell Taylor bubble occupying one or two subchannels did appear.

References

Chisholm, D., 1973. Void fraction during two-phase flow. Journal of Mechanical Engineering Science 15, 235–236.

Golan, L.P., Stenning, A.H., 1969. Two-phase vertical flow maps. In: Proceedings of Symposium on Fluid Mechanics and Measurements Two-Phase Flow Systems, Paper No. 14, Leeds University.

Kawahara, A., Sato, Y., Sadatomi, M., 1997a. The turbulent mixing rate and the fluctuations of static pressure difference between adjacent subchannels in a two-phase subchannel flow. Nuclear Engineering and Design 175, 97–106.

Kawahara, A., Sadatomi M., Sato Y., 1997b. Two-phase turbulent mixing between subchannel in a simulated rod bundle geometry—The effect of the number of gaps between the subchannels. In: Proceedings of 2nd Japanese–German Symposium on Multi-Phase Flow, pp. 55–64.

Kawahara, A., Sadatomi, M., Sato, Y., 1998. Turbulent mixing of both gas and liquid phases between adjacent subchannels in a two-phase annular flow. In: Proceedings of 3rd International Conference on Multiphase Flow, CD-ROM.

Kawahara, A., Sadatomi, M., 2000a. Modeling of void diffusion coefficient in a two-phase subchannel flow. In: Proceedings of 4th JSME–KSME Thermal Engineering Conference, pp. 611–616.

Kawahara, A., Sadatomi, M., Sato, Y., 2000b. Prediction of turbulent mixing rate of both gas and liquid phases between adjacent subchannels in a two-phase slug–churn flow. Nuclear Engineering and Design 202, 27–38.

Lahey Jr., R.T., Shiralkar, B.S., Radcliffe, D.W., Polomik, E.E., 1972. Out-of-pipe sub-channel measurements in a nine rod bundle for water at 1000 psia. In: Hestroni G. et al. (Eds.),. In: Progress in Heat and Mass Transfer, vol. 6. Pergamon Press, London, pp. 345–363.

Ninokata, H., Aritomi, M., Anegawa, T., Sato, Y., Sadatomi, M., Mishima, K., Nishida, K., Yamamoto, Y., Morooka, S., Yabushita, Y., Sou, A., Kamo, H., Kusuno, S., 1997. Development of the NASCA code for prediction of transient BT and post BT phenomena in BWR rod bundles. In: Proceedings of Fourth International Seminar on Subchannel Analysis, pp. 231–265.

Petrunik, K.J., St. Pierre, C.C., 1970. Turbulent mixing rates for air–water two-phase flows in adjacent rectangular channels. The Canadian Journal of Chemical Engineering 48, 123–125.

Rudzinski, K.F., Singh, K., St. Pierre, C.C., 1972. Turbulent mixing for air–water flows in simulated rod bundle geometries. The Canadian Journal of Chemical Engineering 50, 297–299.

Sadatomi, M., Kawahara, A., Sato, Y., 1994. Flow redistribution due to void drift in two-phase flow in a multiple channel consisting of two subchannels. Nuclear Engineering and Design 148, 463–474.

Sadatomi, M., Kawahara, A., Sato, Y., 1995. Turbulent mixing of both gas and liquid phases between subchannels in two-phase hydrodynamic equilibrium flows. In: Celata, G.P., Shah, R.K. (Eds.), Proceedings of 1st International Symposium on Two-phase Flow Modeling and Experimentation 1, pp. 403–409.

Sadatomi, M., Kawahara, A., Sato, Y., 1996a. Axial variation of void fraction in a hydraulically non-equilibrium two-phase flow in a vertical multiple channel. In: Proceedings of the 3rd KSME–JSME Thermal Engineering Conference I, pp. 339–I 344.

Sadatomi, M., Kawahara, A., Sato, Y., 1996b. Prediction of the single-phase turbulent mixing rate between two parallel subchannels using a subchannel geometry factor. Nuclear Engineering and Design 162, 245–246.

Sadatomi, M., Kawahara, A., Sato, Y., 1997. Proceedings of 1997 ASME Fluid Engineering Diversion Summer Meeting, CD-ROM, FEDSM-3557.

Sato, Y., Kawahara, A., Sadatomi, M., 1996. A proposal for treatment of turbulent mixing in a two-phase subchannel flow. Chemical Engineering Communications 141 & 142, 399–413.

Singh, K., St. Pierre, C.C., 1973. Two-phase mixing for annular flow in simulated rod bundle geometries. Nuclear Science and Engineering 50, 382–401.

Sterner, R.W., Lahey Jr., R.T., 1982. Air/water subchannel measurements of equilibrium quality and mass flux distribution in a rod bundle. NUREG/CR-3373, US Nuclear Regulatory Commission.

Taitel, Y., Barnea, D., Duckler, A.E., 1980. Modeling flow pattern transition for steady upward gas–liquid flow in vertical tubes. AIChE Journal 26 (3), 345–354.

Tapucu, A., 1977. Studies on diversion cross-flow between two parallel channels communicating by a lateral slot. I. Transverse flow resistance coefficient. Nuclear Engineering and Design 42, 297–306.

Tapucu, A., Merilo, M., 1977. Studies on diversion cross-flow between two parallel channels communicating by a lateral slot. II. Axial pressure variations. Nuclear Engineering and Design 42, 307–318.

Tapucu, A., Ahmad, S.Y., Gençay, S., 1982. Behavior of two-phase flow in two laterally interconnected subchannels. In: Proceedings of the 7th International Heat Transfer Conference, pp. 361–366.

Venkateswararao, P., Semiat, R., Dukler, A.E., 1982. Flow pattern transition for gas–liquid flow in a vertical rod bundle. Int. J. Multiphase Flow 8, 509–524.

Yadigaroglu, G., Maganas, A., 1995. Equilibrium quality and mass flux distributions in an adiabatic three-subchannel test section. Nuclear Technology 122, 359–372.

Yagi, M., Mitsutake, T., Morooka, S., Inoue, A., 1992. Void fraction distribution in BWR fuel assembly and evaluation of subchannel code. In: Ninokata, H., Aritomi, M. (Eds.), Subchannel Analysis in Nuclear Reactor. The Institute of Applied Energy and Atomic Energy Society of Japan, pp. 141–167.